Journal of Solid State Chemistry **160,** 332–339 (2001)
doi:10.1006/jssc.2001.9237, available online at http://www.idealibrary.com on IDEAL®

Chemical Degradation in Thermally Treated Ferrite/Superconductor Multiphase Materials: Modeling Parameters

Agnes Kopia-Zastawa,*,† I. Suliga,† A. Siwek,† J. Kusinski,† S. Villain,* M. A. Fremy,* M. H. Pischedda,* and J. R. Gavarri*,[1]

*Laboratoire Matériaux Multiphasés et Interfaces (MMI) Faculté des Sciences et Techniques, Université de Toulon-Var, BP 132, 83 957 La Garde, France; and †University of Mining and Metallurgy, 30 Al. Mickiewicza, 30 059 Kraków, Poland
E-mail:gavarri.jr@univ-tln.fr.

Received December 21, 2000; in revised form April 18, 2001; accepted May 11, 2001

Solid state chemical evolutions are studied in the case of superconductor/ferrite composites as a function of time and temperature. Pellets have been fabricated from ferrite $NiFe_2O_4$ and superconducting cuprate $Bi_{1.6}Pb_{0.4}Sr_2Ca_2Cu_3O_{10+X}$ (noted as Bi-2223). Two types of experimental approaches are presented: high-temperature electrical complex impedance spectroscopy, and EDAX analyses performed from scanning electron microscopy. From the in situ electrical analyses, two steps in the solid state chemical evolutions have been evidenced for the first time. They can be associated with two types of solid state reactions: (i) direct reactions between the ferrite phase and the superconducting matrix and (ii) a self-degradation of the superconducting phase probably associated with a homogenization of elements. The electrical analyses are modeled using two types of kinetics parameters. From the EDAX analyses, the local distribution of each element is determined. The concentration profiles found for the various elements (Ni, Fe, Bi, Sr, Ca, Cu) are interpreted in terms of a virtual diffusion law involving virtual D^* coefficients. These coefficients are found to be of about 10^{-11} (cm^2/s) in the range 800–830°C. © 2001 Academic Press

Key Words: **heating process; chemical diffusion; reaction kinetics; ferrite–superconductor composites; impedance spectroscopy; scanning electron microscopy; modeling.**

1. INTRODUCTION

Generally, composite materials are fabricated to improve at least one macroscopic property. In the case of superconductor based composites, many works (1–31) have been carried out in order to improve mechanical properties and chemical behaviors, to modify the electrical responses, or to facilitate the manufacturing processes.

In the present work, we deal with the chemical degradation processes involved in compacted pellets obtained from a powdered $Bi_{1.6}Pb_{0.4}Sr_2Ca_2Cu_3O_{10+X}$ superconducting phase (32) and of ferrite $NiFe_2O_4$ additions. In these materials, we have recently observed specific magneto-resistive behaviors at low temperature (77 K), potentially interesting for new sensor applications.

In our recent work (33), using X-ray diffraction analyses and magnetic measurements, we studied and modeled the degradation of the initial phases $Bi_{1.6}Pb_{0.4}Sr_2Ca_2Cu_3O_{10+X}$ (as the S phase, $T_c = 110$ K) and $NiFe_2O_4$ (as the F phase) in similar composites. These composites, noted S/F, were compacted then sintered at various temperatures and with variable volume fractions of the ferrite. Taking into account a modeling approach of the degradation of initial phases, we have shown that the chemical reactions in these composites were complex, with at least, two types of reaction processes. These two types of reaction processes were assumed to be associated with two different parameters k_1 and k_2 and a noninteger reaction parameter noted n in the chemical reaction:

$$F + n.S \rightarrow P \qquad [1]$$

$$S \rightarrow P'. \qquad [2]$$

Thanks to this semi-empirical approach, we were able to describe the degradation kinetics of the initial phases during the chosen thermal treatment process. Four types of parameters describing the chemical evolution in our composites were defined:

- n—parameter characteristic of the chemical reaction that can be associated with the fast degradation of the Bi-2223 phase
- k_1—kinetics parameter of the degradation rate due to S/F reactions
- k_2—kinetics parameter of the self-degradation of the cuprate phase
- f—weighting parameter associated with the competition between the two degradation processes (33).

[1] To whom correspondence must be addressed.

0022-4596/01 $35.00

However, it is well known that the effective chemical evolution is more complex. We must keep in mind that the effective process involves two different fractions of elements: a first fraction that migrates and a second fraction that forms new stable phases. In addition, the migration itself occurs through two main paths: the diffusion via the crystal lattices (with a limited rate) and diffusion via the grain boundaries or pores (with a higher rate). Precipitation of new phases can occur after the ionic species (or groups of elements) have migrated without reacting along the free interfaces present in such granular solids.

Now, for a better understanding of the chemical reactivity in such two-phase composites, we present a new approach, making use of an in situ electrical analysis. Then using scanning electron microscopy associated with EDAX analyses, we try to interpret the evolution of concentration profiles in terms of virtual diffusion reaction coefficients.

2. EXPERIMENTAL PART

2.1. Sample Preparation

The superconducting phase was an Aldrich powder of bismuth cuprate ($Bi_{1.6}Pb_{0.4}Sr_2Ca_2Cu_3O_{10+X}$), having a standard "offset" transition temperature T_c of 110 K. The ferrite was a commercial powder of $NiFe_2O_4$, obtained from a polish industry specializing in magnetic materials (ZMM-Polfer).

The initial average sizes were controlled using a laser Malvern sizemeter in a polyphase mode analysis. The sizes of the solid particles are analyzed in the range 0.3–300 μm. The mean linear diameters were found to be 5 μm for the Bi-2223 powder and 30 μm for the ferrite powder.

Two types of samples were prepared.

To perform the in situ electrical experiments, the initial composites were firstly prepared by compressing mixtures of powders with 20% volume fractions of ferrite under 5 kbar to obtain pellets of about 13 mm in diameter and about 2 mm in thickness. These samples are prepared at room temperature, to be inserted in the electrical device at a fixed temperature T for a heating time t.

Then to perform local analyses using scanning electron microscopy (SEM), other series were prepared in the temperature range 800 to 840°C at various heating times (5 to 30 min). The final samples selected for the SEM analyses were chosen under the following conditions: initial volume fraction $\Phi(\text{ferrite}) = 0.20$; heating temperatures $T = 800$, 820, and 830°C; heating time $t = 30$ minutes. To obtain statistical determinations, four series corresponding to the same conditions were systematically prepared.

2.2. Electrical Complex Impedance Spectroscopy

To better understand the reaction processes in such samples, a specific thermal analysis involving electrical impedance measurements has been performed. The initial samples were the samples having 20% ferrite, without any thermal treatment.

An electrical complex impedance spectroscopy equipment (Solartron SI 1260 impedance gain phase analyzer) and a high-temperature device were used to follow the high-temperature evolutions of compacted pellets having a fixed initial composition $\Phi(\text{ferrite}) = 0.20$. Three pellets were successively fired at 780, 800, and 820°C in the high-temperature impedance cell.

To describe the reaction and diffusion processes in our composites (heating time of $t = 30$ min) the evolution of the impedance $Z(= Z' + j.Z'')$ was analyzed in the range $t = 0$ to 150 min. In the case of pure resistive samples let us recall that $Z' = R$.

The electrical resistance R of each sample is expected to increase with time: first because of the degradation of the matrix that presents metallic behavior, and, secondly because of the formation of a lot of oxides having insulating or semi-conducting properties.

Each sample was placed in air between silver electrodes, in a homemade high-temperature cell. The working cell can be moved through a cylindrical furnace and quickly subjected to a given temperature T. After a short period of 5 min, each sample is assumed to be under equilibrium. Electrical analyses are then carried out at variable frequencies v, using a frequency range v of 10^{-3} to 10^7 Hz in a first time (first experiment), and then a close frequency range (10^{-1} to 10^6 Hz, and then 10^{-1} to 10^2 Hz), more adapted to the speed of the reaction. The classical Nyquist representations (real part, Z'; imaginary part, $-Z''$) were easily interpreted in terms of vertical lines, characteristic of resistor–inductance equivalent circuits (R and inductance L are in series; $Z_{\text{equiv}} = R + j2\pi L v$). Each resistance $R(t, T)$ was classically obtained by extrapolation from these Nyquist diagrams (intersection with real axis).

2.3. Scanning Electron Microscopy and X-Ray Emission Analyses (EDAX)

The samples subjected to thermal treatments were subjected to local analyses. The scanning electron microscopy analysis was carried out using PHILIPS XL 30 equipment to characterize the distribution of each element before and after heating. Backscattered electron images were used to determine morphology evolutions of ferrite grains and superconducting matrix. Using X-ray emission analysis (EDAX equipment) the local chemical compositions were determined. The analysis of each element is carried out from the center of typical ferrite grain to the superconducting matrix.

The relative concentration of one element Me is a function of a distance r, a time t, and a temperature T. For a fixed heating time t and a fixed heating temperature T, the

concentration profiles $C_{Me}(r, t, T)$ were determined before and after thermal treatments for each series of samples as follows:

- Ferrite grains having isotropic forms and approximate diameters of 30 to 50 μm are systematically chosen to determine concentration profiles.
- The concentrations of the elements are recorded with a focalized electron beam moving from the grain center to the matrix along a line.
- The measurement is reproduced ten times in all plane directions.
- Each concentration profile is independently analyzed and interpreted.
- From the analysis of apparent concentration profiles obtained in the nonsintered samples, it is possible to determine some experimental corrections (edge effects due to electron beam penetration).
- The origin for each diffusion process is extrapolated: it results that after thermal treatment, there is a large uncertainty on the determination of r.
- The concentrations of the elements were calculated using the classical ZAF corrections.

3. RESULTS

3.1. Time Dependence of Electrical Properties

From the experimental data $R(T, t)$, we calculated the conductance $\Sigma(T, t)$:

$$\Sigma(T, t) = \frac{1}{R(T, t)}.$$

According to the experimental data, one can note that for a fixed temperature T, the conductance value $\Sigma(T, t)$ varies with the heating time t.

In Figs. 1a–1c the three evolutions of $\Sigma(T, t)$ are observed: each curve $\Sigma(T, t)$ can be interpreted in terms of two processes with two kinetics parameters. These processes can be directly linked with the two types of reactions previously invoked to model our X-ray data (see (33)). These degradation processes have been recalled in the Introduction. A first type of process might be direct ferrite/superconductor reactions that could occur at low time t during the heating process. A second type of process should be the usual modifications of the superconducting phase itself (self-degradation), which is not stable at these temperatures.

We have modeled the three experimental curves using the function

$$\Sigma(T, t) = \Sigma_0 + \Sigma_1.\exp(-K_1 t^p) + \Sigma_2.\exp(-K_2 t^q).$$

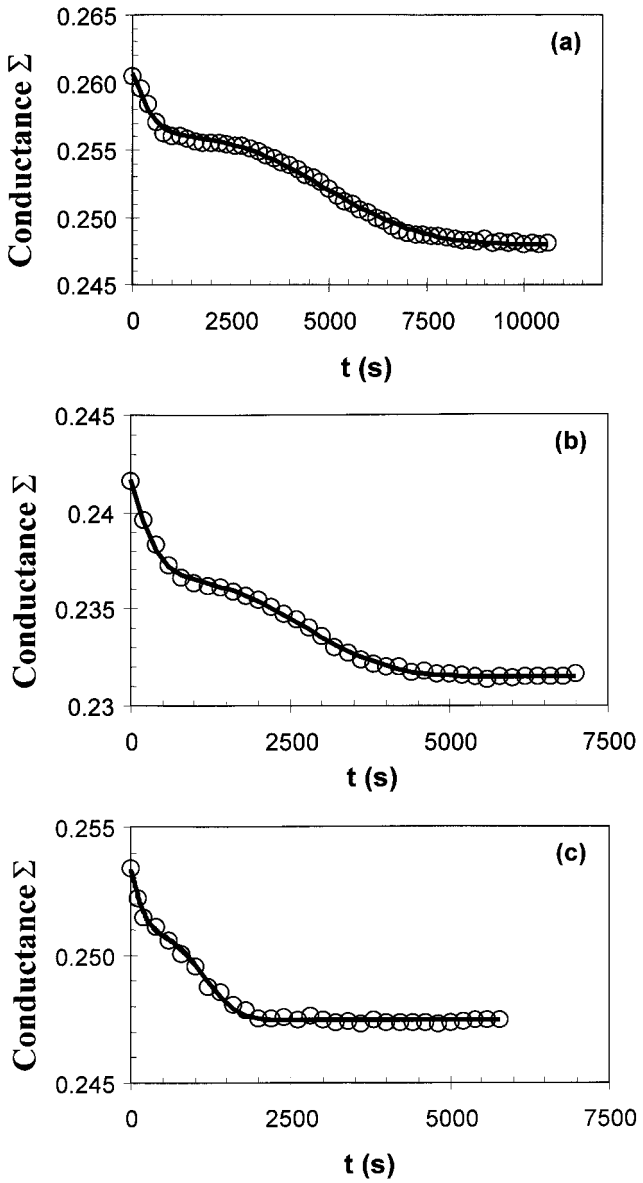

FIG. 1. (a, b, c) Time dependence of the extrapolated conductances $\Sigma(t, T)$ at fixed heating temperatures T and for a fixed initial composition Φ(ferrite) = 0.20. The evolution of $\Sigma(t, T)$ can be associated with a two-step process (direct S/F reaction and S/S self-degradation and phase homogenization), each process being thermally activated: (a) $T = 780°C$, (b) $T = 800°C$, (c) $T = 820°C$.

One can note that at the time $t = 0$ s, we have

$$\Sigma(T, 0) = \Sigma_0 + \Sigma_1 + \Sigma_2,$$

then transformation of the composite can be followed by the term $\Sigma(T, 0) - \Sigma(T, t)$ with

$$\Sigma(T, 0) - \Sigma(T, t) = \Sigma_1.(1 - \exp(-K_1 t^p)) + \Sigma_2.(1 - \exp(-K_2 t^q))$$

in which two evolutions according to Avrami models appear:

—a first term, $\Sigma_{SF}\ (T, t) = \Sigma_1.(1 - \exp(-K_1 t^p)$, describes the S/F transformation

—a second term, $\Sigma_{SS}\ (T, t) = \Sigma_2.(1 - \exp(-K_2 t^q)$, describes the S/S evolution.

In this model, the $\Sigma(T, 0)$ term ($t = 0$) is directly connected with the initial sample: it only depends on the composition and elaboration conditions (compacted pellet before heating).

The $\Sigma_1.\exp(-K_1 t^p)$ and $\Sigma_2.\exp(-K_2 t^q)$ functions depends on kinetics factors (K_1 and K_2) and on exponents p and q characteristic of the degradation process. In the Avrami expression, it has been shown that the parameters p and q depend on the nucleation rate of the new phase, and on the growth process (diffusion controlled, or phase boundary controlled).

Generally, in the case of disordered and heterogeneous media, fractal approaches involve noninteger exponents.

According to Avrami (34–36), these exponents are noninteger: only for a pure first-order reaction (S/F reaction) should the ideal exponent be equal to 1. For a three-dimension diffusion-controlled process, according to Masuda *et al.* [37] and Hulbert *et al.* [38], the exponent should be close to 3.

The refined parameters are reported in Table 1. They are characteristic of thermally activated processes.

In Figs. 1a–1c the calculated curves (straight lines) have been represented: it can be concluded that the proposed model fits very well the experimental data (large circles).

From Table 1, it clearly appears that the two processes (S/F and S/S reactions) previously considered in our modeling approach can directly be linked with the parameters Σ_1, Σ_2, K_1, and K_2.

We can note that the $\Sigma(T, 0)$ value for $T = 800°C$ presents an anomaly. It is clearly smaller than the value observed at $T = 780$ and 820°C: even if the composition of these three composites should be the same, we should admit that the distribution of the phases in the pellets might not be the same in all the samples.

TABLE 1
Refined Parameters Obtained from the Experimental Data at 780, 800, 820°C (Vol. Fraction of Ferrite: 0.20)

	T			
	780°C	800°C	820°C	Comments
Σ_0	247×10^{-3}	231×10^{-3}	247×10^{-3}	
Σ_1	4.6×10^{-3}	5.2×10^{-3}	2.5×10^{-3}	
Σ_2	8.1×10^{-3}	5.0×10^{-3}	3.3×10^{-3}	$E_a = 144$ kJ/mol
$\Sigma_0+\Sigma_1+\Sigma_2$	259.7×10^{-3}	241.2×10^{-3}	253.8×10^{-3}	$E_a = 215$ kJ/mol
K_1	0.7×10^{-3}	1.1×10^{-3}	1.4×10^{-3}	$E_a = 166$ kJ/mol
K_2	0.6×10^{-11}	1.6×10^{-11}	6.5×10^{-11}	$E_a = 569$ kJ/mol
p	1.19	1.17	1.22	Mean value: 1.19
q	2.99	3.09	3.29	Mean value: 3.12

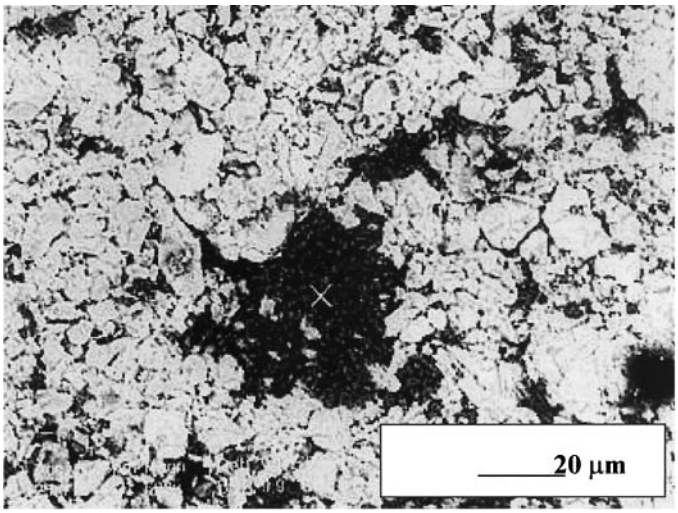

FIG. 2. Micrograph of a standard sample (20% ferrite/80% superconductor) observed before thermal treatment. In black, the ferrite phase. In gray–white the matrix S grains. No modification is observed at the interface S/F.

The activation energies found for K_1 and K_2 are of about 1.7 and 5.9 eV respectively.

The refined values of the exponents are in full agreement with the predictions: p is close to 1 (first-order reaction) and q is close to 3, which is in good accordance with the Avrami models. This means that, as expected, the first process can be associated with a reaction process (first-order reaction), and the second process is strongly associated with a diffusion process: the phase evolution is controlled by the diffusion of migrating species in a 3D disordered medium.

3.2. Concentration Profiles

In Figs. 2 to 5, selected micrographs obtained from backscattered electrons and concentrations C of elements obtained from EDAX measurements are presented.

In each micrograph, the ferrite phase grains appear in black. The granular white of gray grains of the S phase (or the resulting degradation products) surround them. At the ferrite/matrix interface, an intermediate zone (enveloping shell) can be observed. It is the result of the reaction between the S and F phases.

To control the initial morphologies of both superconducting and ferrite phases, SEM analyses were systematically performed before any thermal treatment.

In Fig. 2, we report one micrograph obtained before any thermal treatment (on a 20% sample). The ferrite black grain has no envelope. The white matrix grains present regular forms.

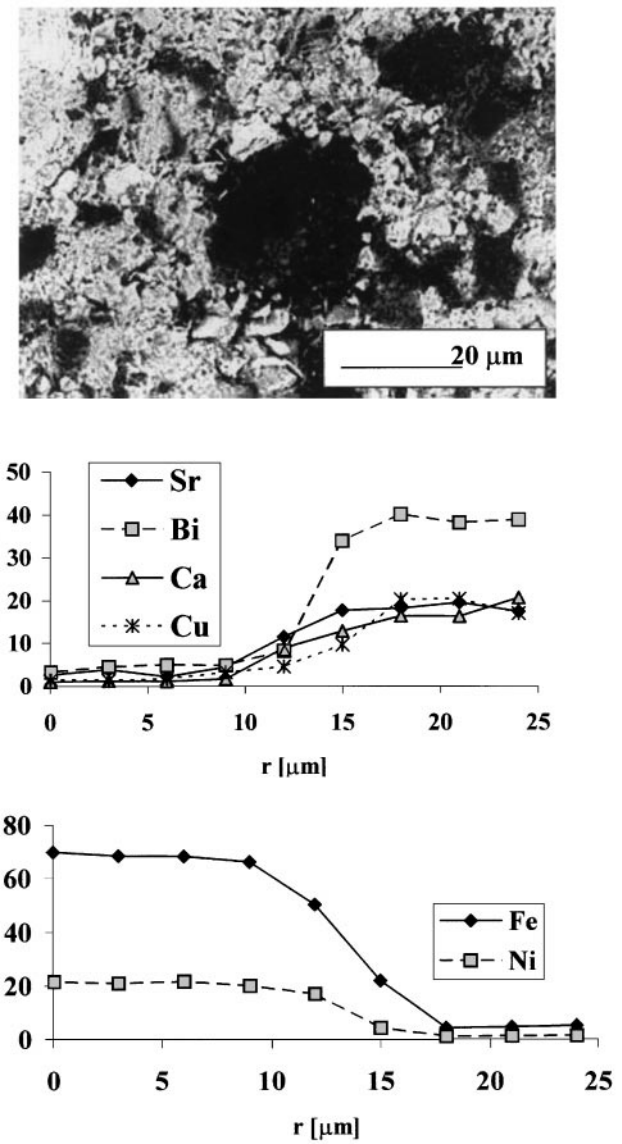

FIG. 3. Interface diffusion and reactions in a quenched sample: Φ(ferrite) = 0.20; $T = 800°C$. Atomic fractions $C(r, t, T)$ are reported as a function of the distance r (in μm) for $t = 1800$ s and $T = 800°C$. In the micrograph, the grain sizes are smaller than in the sample prepared without any heating. The degradation of the ferrite/matrix interfaces occurs. The matrix grains also degrade. Two types of degradation process are observed.

In the micrographs of Figs. 3 to 5, it can be clearly observed that there is a strong evolution of the grain morphologies of both S and F phases as a function of temperature. In Fig. 3 ($T = 800°C$), as the initial morphologies observed in Fig. 2 can be considered as standard morphologies (time $t = 0$), the S grain morphologies observed far from one isolated ferrite grain are weakly modified. As could be expected, when the temperature increases (Figs. 4 and 5), there is a clear size decrease linked to the degradation of this S phase.

Let us recall that, in the well-known equilibrium diagram established by the authors (32), this cuprate phase is only stabilized in the temperature range 857 to 876°C. This means that below the temperature of 857°C, the degradation of the S phase necessarily occurs. Obviously, the kinetics of such a process is thermally activated. This is the case in our experiments. However, this evolution is also accelerated by the presence of the additional ferrite phase. This is well confirmed in our Figs. 3 to 5.

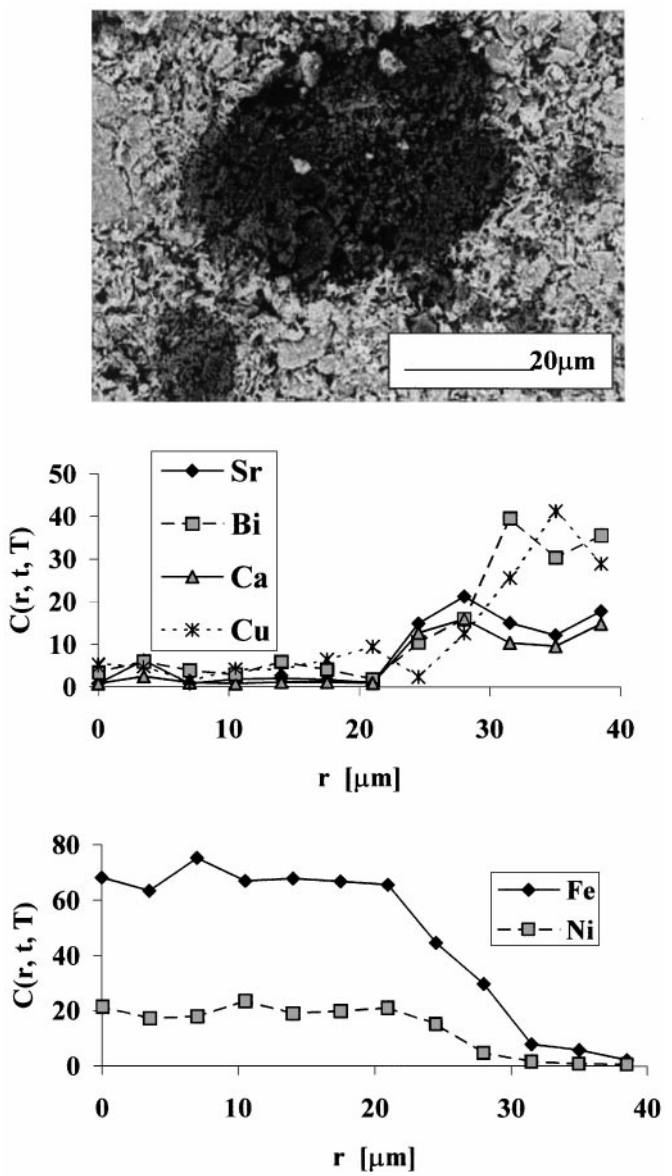

FIG. 4. Interface diffusion and reactions in a quenched sample: Φ(ferrite) = 0.20; $T = 820°C$. Atomic fractions $C(r, t, T)$ are reported as a function of the distance r (in μm) for $t = 1800$ s and $T = 820°C$. In the micrograph, the grain sizes are smaller than in the sample sintered at 800°C. Increased degradation is observed at the ferrite/matrix interfaces. The matrix grains also degrade. The two types of degradation process are confirmed.

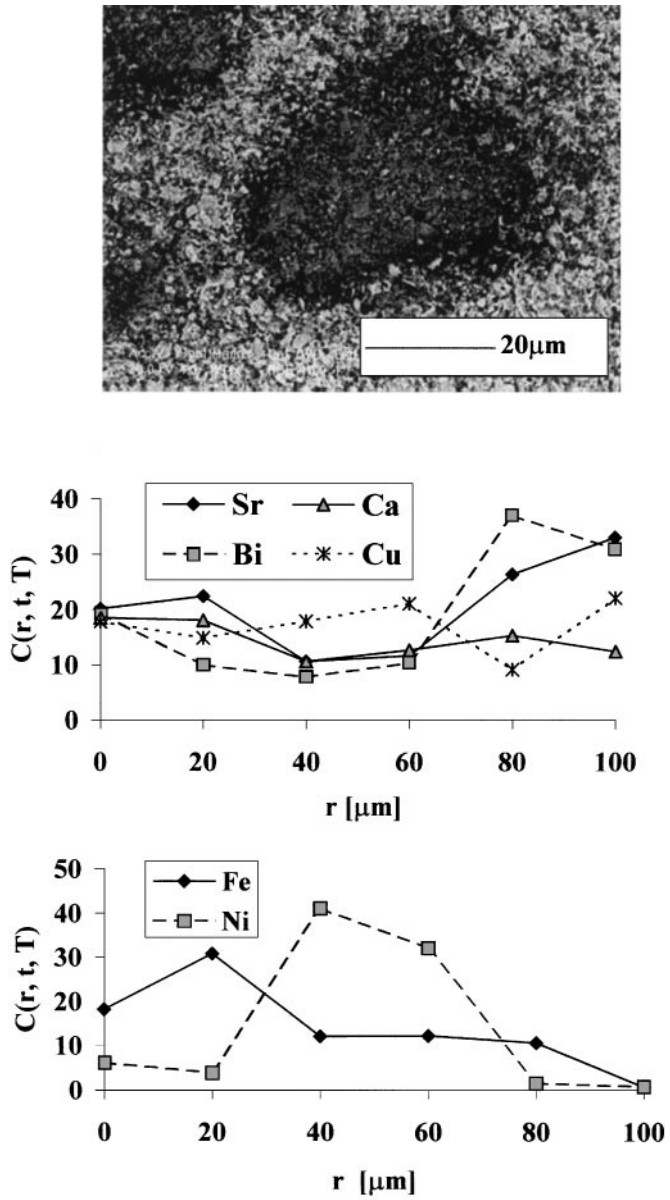

FIG. 5. Interface diffusion and reactions in a quenched sample: Φ(ferrite) = 0.20; $T = 830°C$. Atomic fractions $C(r, t, T)$ are reported as a function of the distance r (in μm) for $t = 1800$ s and $T = 830°C$. In the micrograph, the grain sizes have strongly decreased: a pronounced degradation of both matrix and ferrite is clearly observed.

Finally, in Figs. 3 to 5 the two degradation processes can be clearly associated with the two types of morphologies observed: (i) close to a ferrite grain (S/F reaction) and (ii) far from this ferrite grain (S degradation).

3.2.1. Approximate model: Virtual Fick law. It is well known that in the case of diffusion of reactants, the general solution for diffusion–reaction processes is highly complex (39).

If we express the Fick equation as

$$\partial C^*/\partial t = D\Delta C^* - KC^*, \qquad [3]$$

it is possible to show that the solution $C^*(r, t, T)$ in presence of reaction ($K > 0$) is

$$C^*(r, t, T) = C_{(K=0)} \exp(-Kt) + K \int_0^t C_{(K=0)} \exp(-Kt)\, dt < C_{(K=0)}, \qquad [4]$$

where the $C_{(K=0)}$ function is the ideal solution of the equation for $K = 0$.

Such a solution (4) is difficult to compute. In addition, taking into account the large uncertainties in the data, a complex mathematical treatment should be excessive.

So, we have chosen to define approximate "virtual" diffusion coefficients and to fit a simplified model to the data.

The approximation can be justified from the basic definition of flux

$$J = -D\,\mathrm{grad}(C) \qquad [5]$$

in which the C function generally depends on the initial number of particles N_0 (at the origin). In our system, as reactions occur with diffusion, the effective concentrations C^* are weaker than the concentrations calculated from ideal diffusion laws ($C^* < C$). At a fixed distance r_1 from the center of diffusion, the effective concentrations result from the apparent decrease in particle flux, due to phase formations (for $r < r_1$), compensated by a part of precipitation at $r = r_1$ due to local reactions. As shown in the specific solution reported above (relation [4]), the effective concentrations at this distance are conditioned by reaction kinetics parameters and chemical diffusion coefficients of the classical Fick law.

The effect of temperature is to activate both diffusion (D) and chemical reactions (K parameter). To obtain a simplified representation of the mathematical solution, we have chosen to use the solution for $K = 0$ (C function) and to consider the D^* coefficient as an empirical term associated with reaction and diffusion.

Using this empirical function (C), the complex thermal activation may be expressed from the unique virtual D^* coefficient assumed to be composed of two contributions (D for diffusion, R for reaction):

$$D^* = D.R \qquad [6]$$

$$D = D_0 \exp(-E_D/RT) \qquad [7]$$

$$R = R_0 \exp(-E_R/RT). \qquad [8]$$

Now, such a virtual D^* term is thermally activated with two energy contributions:

$$E_A = E_D + E_R. \qquad [9]$$

3.2.2. Corrections for element distributions. For a better interpretation of the observed concentration profiles, it has been necessary to analyze the compacted samples (in form of pellets) before any heating process. The main feature resides in the fact that the initial concentration profiles systematically present sigmoid aspects at the ferrite/matrix interfaces: this is due to edge effects for electron beam penetration and irregular shapes of grains. These initial profile are similar to diffusion profiles and must be taken into account.

3.2.3. Virtual diffusion model. To choose a model sufficiently representative of our complex system, the following hypotheses were assumed:

- the process of chemical diffusion goes in two reverse directions
- the elements diffuse according to a virtual Fick law
- the diffusion coefficients of the particular elements do not depend on the concentration of the other elements
- the distances between grains are large enough to omit the influence of other grains
- the model will be limited to a spherical diffusion from a distribution of four spheres with fixed radii r_m ($m = 1, 4$): the extreme radii are adapted to simulate the initial concentration profile ($r_1 - r_3 = 5$ μm).

The chosen model for one isolated sphere is (40)

$$c = \frac{c_0}{2}\left[\operatorname{erf}\left[\frac{r_m - r}{2\sqrt{Dt}}\right] + \operatorname{erf}\left[\frac{r_m + r}{2\sqrt{Dt}}\right] + \frac{2\sqrt{Dt}}{r\sqrt{\pi}}\left\{\exp\left[-\frac{(r + r_m)^2}{4Dt}\right] - \exp\left[-\frac{(r_m - r)^2}{4Dt}\right]\right\}\right],$$

where r is the distance from the ferrite grain center, r_m is the radius of one sphere, D^* is the virtual diffusion coefficient, t is the heating time, and c_0 is a constant composition fitted to the data.

So, we have considered that each ferrite grain could be described in terms of a superposition of spherical atom distributions. The total concentration could be simulated by a sum of four spheres. The total concentration C will be $C = \frac{1}{4}[c_1 + c_2 + c_3 + c_4]$.

4. DISCUSSION

In Table 2 the calculations of the D^* coefficients and of the activation energies E^* are reported.

As shown in this table, the largest D^* coefficients are observed for the Ni ions. The Sr, Ca, and Cu ions also move quickly: this was expected because the Bi-2223 phase itself is not stable in this temperature range. The Fe ions seem to migrate more slowly: this can be interpreted in terms of formation of the very stable refractory phase Fe_2O_3 (observed in X-ray diffraction patterns). For the constituents of the bismuth cuprate, a stabilization of the migration rates seems to be observed in the range 820–830°C (that is not the case for the Fe and Ni elements). This is directly due to the fact that element homogenization needs a longer time for the minor ferrite phases than for the major Bi-2223 phases.

Mean values of the reaction–diffusion coefficients have been calculated. These mean values take into account the atom fractions in the composites. Using all atoms with their relative fractions, a D_{SF} mean value has been defined: it should represent the S/F diffusion–reaction. Using the sole bismuth cuprate atoms, a D_{SS} mean value has been calculated: it delivers some indication of the cuprate evolution.

These D_{SF} and D_{SS} values are reported in Table 3.

5. CONCLUSION

The chemical evolutions in F/S composites have been described and interpreted using two types of complementary macroscopic and local approaches. For the first time, a two-step reaction–diffusion process characteristic of these multiphase systems has been clearly observed and modeled. Two types of models have been used to interpret the data. A first semi-empirical model has been proposed to interpret the electrical measurements. A second model making use of a virtual Fick law has been developed to propose virtual diffusion coefficients.

TABLE 2
Virtual Reaction–Diffusion Coefficients D^* of Each Element (Calculated from the Model)

Temperature (°C)	$D_{Fe} * 10^{-11}$ (cm^2/s)	$D_{Ni} * 10^{-11}$ (cm^2/s)	$D_{Bi} * 10^{-11}$ (cm^2/s)	$D_{Sr} * 10^{-11}$ (cm^2/s)	$D_{Ca} * 10^{-11}$ (cm^2/s)	$D_{Cu} * 10^{-11}$ (cm^2/s)
800	1.56	0.62	3.83	2.04	3.75	3.1
820	4.84	2.04	5.79	9.05	6.21	9.16
830	6.03	7.14	6.64	9.05[a]	6.21[a]	16.5
E (kJ/mol)						
800–830°C	459	767	183	524	177	545

[a]These values are abnormal, see text.

TABLE 3
Values of the Mean Virtual Reaction–Diffusion Coefficients *D

Temperature (°C)	$D_{SF} * 10^{-11}$ (cm^2/s)	$D_{SS} * 10^{-11}$ (cm^2/s)
800	2.21	3.17
820	5.82	7.73
830	8.38	10.4
E_A ($kJ.mol^{-1}$)	442	395

○ From the time-dependent electrical analyses and the semi-empirical model, it has been possible to determine two kinetics coefficients K_1 and K_2 associated with two types of reactions (S/F reaction and S/S self-degradation). This confirms the model previously proposed in (33). These coefficients are thermally activated with activation energies of about 1.72 and 5.9 eV respectively.

○ From the semi-empirical model, it results that two types of noninteger exponents, p and q, can be defined. The calculated exponents are in full agreement with the Avrami model (36–38): they confirm our initial description of the degradation two-step process.

○ The individual values of the diffusion coefficients are found to be in the range 0.6 to 16 10^{-11} cm^2/s.

○ The activation energies found for individual elements, range between 1.7 and 7 eV.

Now, these new results will be helpful in optimizing the thermal treatments of our composites and in improving their magneto-resistive properties: a detailed study of the magneto-resistive behaviors of these S/F composites is in progress and will be published later.

REFERENCES

1. S. Jin, R. C. Sherwood, T. H. Tiefel, G. W. Kammlott, R. A. Fastnacht, M. E. Davis, and S. M. Zahurak, *Appl. Phys. Lett.* **52,** 1628 (1988).
2. M. Manzel, L. Illgen, and R. Hergot, *Phys. Stat. Sol.* (*A*) **117,** K119 (1990).
3. L. S. Hung, J. A. Agostinelli, G. R. Par-Pujalt, and J. M. Mir, *Appl. Phys. Lett.* **53,** 2450 (1988).
4. W. Gao and J. B. Vander Sande, *Physica C* **171,** 69 (1990).
5. R. H. Arendt, M. F. Garbauskas, K. W. Lay, and J. E. Tkaczyk, *Physica C* **194,** 383 (1992).
6. W. Gao and J. B. Vander Sande, *Mater. Sci. Eng. B* **10,** 247 (1990).
7. Y. Huang, G. F. De la Fuente, and A. Sotelo, *Physica C* **185–189,** 2401 (1991).
8. Y. Ishida, J. Matsuzaki, T. Kizuka, and H. Ichionose, *Physica C* **190,** 67 (1991).
9. J. Koshy, K. S. Kumar, Y. P. Yadava, and A. D. Damodaran, *J. Mater. Sci. Lett.* **13,** 554 (1994).
10. Y. D. Chiu, T. S. Lei, and C. H. Kao, *J. Mater. Sci.* **29,** 2678 (1994).
11. R. Chaim and Y. Ezer, *J. Mater. Sci.* **28,** 4205 (1993).
12. R. Chaim and Y. Ezer, *J. Mater. Sci.* **28,** 5007 (1993).
13. R. Chaim and Y. Ezer, *J. Mater. Sci.* **28,** 4273 (1993).
14. In-Gan Chen, S. Sen, and D. M. Stefanescu, *Appl. Phys. Lett.* **52,** 1355 (1988).
15. G. Xiao, F. H. Streitz, M. Z. Cieplak, A. Bakhshai, A. Gavrin, and C. L. Chien, *Phys. Rev. B* **38,** 776 (1988).
16. R. K. Nkum, A. Punnett, and W. R. Datars, *Physica C* **202,** 371 (1992).
17. C. Veerender and M. Nagabhooshanam, *J. Mater. Sci.* **30,** 369 (1995).
18. Y. Li and B. Yang, *J. Mater. Sci. Lett.* **13,** 594 (1994).
19. Y. Nishi, K. Nozaki, T. Kurotaki, Y. Kita, and K. Oguri, *J. Mater. Sci. Lett.* **11,** 1211 (1992).
20. Y. Nishi, K. Nozaki, T. Kurotaki, Y. Kita, and K. Oguri, *Phys. Lett. A* **163,** 465 (1992).
21. B. Ropers, F. Carmona, and S. Flandrois, *Physica C* **204,** 71 (1992).
22. B. Ropers, F. Carmona, and S. Flandrois, *Appl. Supercond.* **1,** 1015 (1993).
23. S. Dubois, S. Flandrois, and F. Carmona, *Physica A* **207,** 265 (1994).
24. A. Ouammou, O. Pena, A. Benlhachemi, J. R. Gavarri, and C. Carel, *Ann. Chim. Fr.* **19,** 493–498 (1994).
25. A. Benlhachemi, J. R. Gavarri, Y. Massiani, and J. Marfaing, *Ann. Chim. Sci. Matér.* **20,** 335–344 (1995).
26. C. Alfred-Duplan, J. Marfaing, G. Vacquier, A. Benlhachemi, J. Musso, and J. R. Gavarri, *Matter. Sci. Eng. B* **29,** 1 (1996).
27. A. Benlhachemi, S. Golec, and J. R. Gavarri, *Physica C* **209,** 353–361 (1993).
28. A. Benlhachemi, J. Musso, J. R. Gavarri, C. Alfred-Duplan, and J. Marfaing, *Physica C* **230,** 246–254 (1994).
29. A. Benlhachemi, J. R. Gavarri, J. Musso, C. Alfred-Duplan, and J. Marfaing, *Metall. Foundry Eng.* **20,** 205–216 (1994).
30. A. Benlhachemi, J. R. Gavarri, Y. Massiani, and S. Aïtyazza, *Physica C* **235–240,** 1511 (1994).
31. A. Siwek, I. Suliga, M. H. Pischedda, J. R. Gavarri, and St. Jasienska, *Solid State Ionics* **80,** 45–52 (1995).
32. J. Schneck, J. C. Toledano, L. Pierre, A. Litzler, D. Morin, J. Primot, H. Savary, and C. Daguet, *J. Less-Comm. Met.* **164/165,** 545–552 (1990).
33. A. Kopia, J. R. Gavarri, I. Suliga, M. A. Fremy, M. H. Pischedda, and St. Jasienska, *J. Solid State Chem.* **145,** 317–326 (1999).
34. M. Avrami, *J. Chem. Phys.* **7,** 1103–1112 (1939).
35. M. Avrami, *J. Chem. Phys.* **8,** 212–224 (1940).
36. M. Avrami, *J. Chem. Phys.* **9,** 177–184 (1941).
37. Y. Masuda, *Thermochim. Acta* **282/283,** 43–49 (1996).
38. S. F. Hulbert, *J. Br. Ceram. Soc.* **6,** 11 (1969).
39. P. W. Atkins, "Physical Chemistry." Oxford Univ. Press, Oxford (1990).
40. W. Joszt, "Diffusion in Solids, Liquids, Gases." Addeneum, New York (1960).